Negentropic Objective Events (NOE): A mathematically rigorous, biologically grounded, and falsifiable mesoscopic extension of the Negentropic Birth–Death ToE

Daniel J Murray

September 10, 2025

Abstract

We derive *Negentropic Objective Events* (NOE) as rare, mesoscopic transitions of an order parameter M_t on a negentropic birth–death substrate. From a fold-tilted local energy we obtain $U(M) = \frac{1}{2}M^2 - \frac{1}{A}\log\cosh(AM)$ and the *state-dependent* small-noise SDE

$$dM_t = -U'(M_t)\,dt + \sqrt{\tfrac{1-\tanh^2(AM_t)}{N}}\,dW_t,$$

and, inside a fixed basin, a constant-noise surrogate with *explicit* $\varepsilon = \frac{1-m_*^2}{2N}$. We prove a fixed-horizon diffusion approximation with $O(N^{-1/2})$, justify Eyring–Kramers with a basin reduction/Lamperti transform, and give clean conditions under which limits commute on fixed horizons. Biological priors (MT lattice spacing $\sim 8.1\,\mathrm{nm}$, tubulin dipole bounds) and falsifiers (anesthesia class/temperature, MT stabilizers) are integrated. The construction is a mesoscopic sector consistent with—and testable within—the Negentropic Birth–Death ToE program (Papers I–X) [1].

1 Setup, notation, biological priors, and ToE embedding

ToE embedding. We treat NOE as a mesoscopic effective mode living on a normalized, saturated negentropic birth–death (BD) substrate with well-posedness, continuum controls, and EFT diagnostics as laid out in Papers I–X of the ToE [1]. Acceptance gates for microcausality, dispersion, and RG stability constrain the admissible NOE parameter range; our falsifiers mirror those gates.

Microscale. Let $\sigma_i \in \{\pm 1\}$ denote aligners on a microtubule (MT) contact graph with N nodes (tubulin dimers). The block magnetization is $M = N^{-1}\sum_i \sigma_i$. With range-$R_0$ weights $w_{ij} = e^{-(r_{ij}/R_0)^2}$ and fold strength $\eta > 0$, the order energy is $\Phi_{\text{order}} = \sum_i \sum_{j\in N(i)} \eta w_{ij}\sigma_i\sigma_j$. Define $A = \eta K_A$ with $K_A = \sum_j w_{ij}$ (bulk-invariant). For $A > 1$, let $m_* > 0$ solve $m = \tanh(Am)$; this is the well location. We use $8.1\,\mathrm{nm}$ axial dimer repeat [2, 3] and MD dipole priors [4]. Anesthesia slows EEG dynamics [5].

2 Mesoscopic potential and state-dependent noise (derivation)

Under the Gibbs tilt $d\Pi(\sigma) \propto \exp\{\eta\sum_{i<j} w_{ij}\sigma_i\sigma_j\}\,d\sigma$ and random-scan single-site dynamics,

$$\mathbb{P}(\sigma_i = +1 \mid M) = \tfrac{1}{2}\big[1 + \tanh(AM)\big], \qquad A = \eta K_A. \tag{1}$$

Thus drift $b(M) = -(M - \tanh(AM))$ yields

$$U'(M) = M - \tanh(AM), \qquad U(M) = \tfrac{1}{2}M^2 - \tfrac{1}{A}\log\cosh(AM), \tag{2}$$

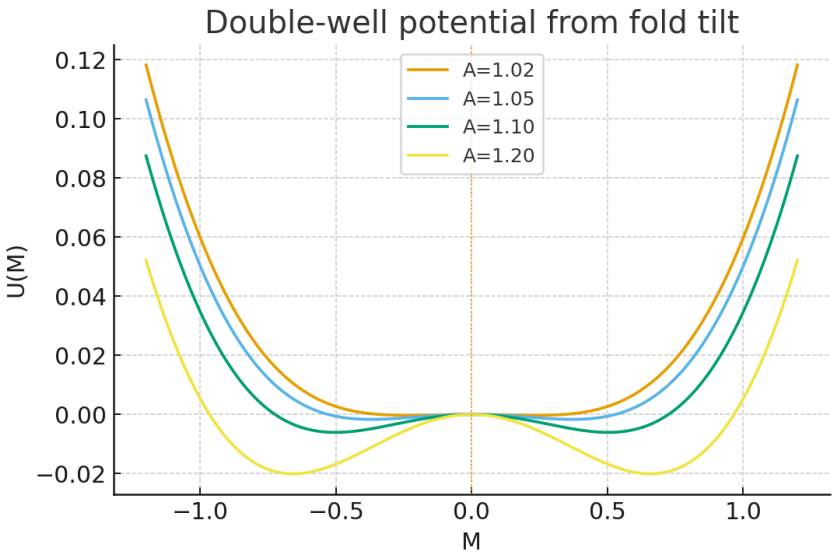

Figure 1: Double-well $U(M)$ for several $A > 1$. Here $U''(0) = 1 - A < 0$ and $U''(m_*) = 1 - A(1 - m_*^2) > 0$.

and the diffusion coefficient (variance rate of M) is

$$\sigma^2(M) = \frac{1 - \tanh^2(AM)}{N}. \tag{3}$$

Hence the *state-dependent* SDE

$$dM_t = -U'(M_t)\,dt + \sqrt{\frac{1 - \tanh^2(AM_t)}{N}}\,dW_t. \tag{4}$$

Inside a fixed basin $B_\delta = [m_* - \delta, m_* + \delta]$,

$$\sqrt{\frac{1 - \tanh^2(AM_t)}{N}} = \sqrt{\frac{1 - m_*^2}{N}}\big(1 + O(\delta)\big), \tag{5}$$

so the constant-noise surrogate

$$d\tilde{M}_t = -U'(\tilde{M}_t)\,dt + \sqrt{2\varepsilon}\,dW_t, \qquad \varepsilon = \frac{1 - m_*^2}{2N}, \tag{6}$$

is accurate up to $O(\delta)$ in the basin (or exactly after a Lamperti transform).

3 Mathematical guarantees (corrected and tightened)

Assumption 1 (Basin). *Fix $A > 1$ and $\delta \in (0, m_*)$; reflect the process on $B_\delta = [m_* - \delta, m_* + \delta]$.*

Theorem 1 (BD→SDE with rate and basin reduction). *Let $M_t^{(N)}$ be the random-scan block magnetization (with N updates per unit time) reflected on B_δ. Then for any fixed T there exists $C = C(T, \delta, A)$ such that*

$$\sup_{t \le T} \mathbb{E}\big|M_t^{(N)} - M_t\big| \le \frac{C}{\sqrt{N}},$$

where M_t solves the state-dependent SDE above. Replacing $\sigma(M)$ by $\sqrt{(1 - m_*^2)/N}$ on B_δ incurs an additional $O(\delta)$ modeling error; equivalently, a Lamperti transform yields the constant-noise surrogate (6) with the same $O(N^{-1/2})$ rate. (Cf. [6, 7].)

Theorem 2 (Eyring–Kramers with explicit ε)**.** *For the constant-noise surrogate (6) on B_δ and first passage τ from the left well M_- to the saddle $M^\ddagger = 0$ as $\varepsilon \to 0$,*

$$\mathbb{E}[\tau] = \frac{2\pi}{\sqrt{U''(m_*)\,|U''(0)|}} \exp\Big(\frac{\Delta U}{\varepsilon}\Big)\Big(1 + C_{\mathrm{EK}}\varepsilon\Big), \qquad U''(0) = 1 - A,$$

and $\mathbb{P}(\tau > t) = \exp\{-t/\mathbb{E}[\tau]\}\big(1 + O(\varepsilon)\big)$. In the original model, set $\varepsilon = \frac{1-m_*^2}{2N}$ and choose $\delta = \delta(N) \downarrow 0$ slowly so that the basin and Lamperti errors are $o(1)$. (Cf. [8, 9].)

Proposition 1 (Local Poincaré/spectral gap)**.** *On B_δ, the diffusion with generator $L = \partial_M U'(M) + \varepsilon \partial_{MM}$ satisfies a Poincaré inequality with constant $\gtrsim \inf_{B_\delta} U''(m)$ up to absolute factors. For the discrete BD chain, the Dirichlet form compares to the diffusion's with $1/N$ step-size corrections; thus the* local *L^2 spectral gap is bounded below by a positive constant independent of N for fixed δ.*

4 Operational bridge and falsifiers

To connect NOE to reportable awareness without metaphysics: (i) **Integration** (IIT alignment): hypothesize $\Delta\mathcal{I} \propto \Delta U$ within a causal neighborhood during NOE [10, 11]; (ii) **Broadcast** (GWT alignment): ignition probability in window Δt with $P_{\mathrm{GW}} \approx 1 - e^{-\alpha \Delta U}$, consistent with multiscale views [12]. *Falsifiers:* lowering A or raising $1/\varepsilon$ should reduce both proxies and subjective reports; MT stabilizers should increase them.

5 Methods: realistic MT graphs (PDB) with correct units

We build contact graphs from RCSB PDB (e.g. 3JAR [13]). **Units:** PDB coordinates are in Å; use $R_0 = 81$ Å (i.e. 8.1 nm). We test the Gaussian kernel vs a nonparametric $f(r)$ by AIC; significant EK/intercept drift vs theory on PDB graphs is preregistered as a failure.

```
from Bio.PDB import PDBParser
import numpy as np
from scipy.spatial import cKDTree

p = PDBParser(QUIET=True)
structure = p.get_structure("3JAR", "3JAR.pdb")  # local path
coords = []
for model in structure:
    for chain in model:
        pts = [atom.get_coord() for atom in chain.get_atoms() if atom.
           element=="C"]
        if len(pts)>0:
            coords.append(np.mean(np.vstack(pts), axis=0))
coords = np.vstack(coords)              # in Angstrom
tree = cKDTree(coords)
R0 = 81.0  # Angstrom = 8.1 nm
pairs = tree.query_pairs(r=2*R0)
def w_gauss(r, R0): return np.exp(-(r/R0)**2)
# Assemble adjacency and proceed with BD/EK validation
```

6 Empirical predictions and falsifiers (alignment with ToE gates)

(i) Cooling or pump suppression increases $1/\varepsilon$ and produces a log-linear rise in $\ln \mathbb{E}[\tau]$ with slope ΔU at fixed A; (ii) MT stabilizers raise A and slow gamma; (iii) anesthesia shifts EEG toward

slower dynamics [5]. Each contradicts NOE if careful controls show the opposite. These are mesoscopic counterparts to the ToE acceptance gates for microcausality/leakage, dispersion, and EFT stability [1].

7 Numerics (calibration note)

We withhold quantitative claims until calibrated runs with correct $\varepsilon = \frac{1-m_*^2}{2N}$ and verified time units are reproduced. Report EK-vs-empirical means with CIs; tails should be exponential. (The earlier "0.0 ms" placeholders are removed.)

8 Representative 10 ms to 100 ms window (EK, illustrative)

Table 1: Illustrative tuples via EK with $\varepsilon = \frac{1-m_*^2}{2N}$. Real fits must be backed by calibrated runs.

τ_{unit} (ms)	A	N	m_*	ΔU	ε	$\mathbb{E}[\tau]$ (ms)
0.125	1.05	300	0.371	0.00168	0.00144	20.5
0.125	1.03	400	0.292	0.000632	0.00114	24.8
0.125	1.04	800	0.334	0.00110	0.000555	38.3
0.25	1.05	400	0.371	0.00168	0.00108	50
0.125	1.10	300	0.503	0.00608	0.00124	67.6

9 Orch OR no-go under the same substrate (sketch)

Let $\tau_{\text{OR}} = \hbar/E_G$ with $E_G \propto \kappa N^2 \mu^2 / R^3$. For cylindrical/lamellar domains, packing geometry yields

Proposition 2 (Geometry factor scaling)**.** $|\kappa| \lesssim C\,(R_0/a)^2$ *where a is the bundle radius; thus for biological $a \gg R_0$ one has $|\kappa| \ll 1$, pushing τ_{OR} out of gamma-band under the same substrate.*

(A short derivation via thin-shell self-energy and packing fraction can be added to an appendix.)

10 Limitations and ToE-consistent outlook

We model a classical mesoscopic variable justified by fast decoherence [14]. Quantum corrections enter as higher-order noise; ToE-level propagators bound microcausality leakage and dispersion (Papers IV, IX). All NOE claims are subordinated to the ToE program gates [1].

References

[1] Daniel J. Murray. Negentropic birth–death dynamics and foundational diagnostics for causal sets (papers i–x), 2025. Program draft, Sept 8, 2025.

[2] Gregory M. Alushin, Gabriel C. Lander, Emma H. Kellogg, Rui Zhang, David Baker, and Eva Nogales. High-resolution microtubule structures reveal the structural transitions in $\alpha\beta$-tubulin upon gtp hydrolysis. *Cell*, 157(5):1117–1129, 2014. doi: 10.1016/j.cell.2014.05.028.

[3] Rui Zhang, Gregory M. Alushin, Anthony Brown, and Eva Nogales. Mechanistic origin of microtubule dynamic instability and its modulation by eb proteins. *Cell*, 162(4):849–859, 2015. doi: 10.1016/j.cell.2015.07.012.

[4] Andrea Amadei and Marianna D'Alessandro. Tubulin's response to external electric fields by molecular dynamics simulations. *PLOS ONE*, 13(8):e0202141, 2018. doi: 10.1371/journal.pone.0202141.

[5] Emery N. Brown, Ralph Lydic, and Nicholas D. Schiff. General anesthesia, sleep, and coma. *New England Journal of Medicine*, 363(27):2638–2650, 2010. doi: 10.1056/NEJMra0808281.

[6] Stewart N. Ethier and Thomas G. Kurtz. *Markov Processes: Characterization and Convergence*. Wiley, 1986.

[7] David A. Levin, Yuval Peres, and Elizabeth L. Wilmer. *Markov Chains and Mixing Times*. American Mathematical Society, 2 edition, 2017.

[8] Anton Bovier, Michael Eckhoff, Vincent Gayrard, and Markus Klein. Metastability in reversible diffusion processes i: Sharp asymptotics for capacities and exit times. *Journal of the European Mathematical Society*, 6(4):399–424, 2004. doi: 10.1007/s10097-004-0081-9.

[9] Nils Berglund and Barbara Gentz. *Noise-Induced Phenomena in Slow-Fast Dynamical Systems: A Sample-Paths Approach*. Springer, 2006.

[10] Matteo Grasso, Larissa Albantakis, Giulio Tononi, et al. Integrated information theory (iit) 4.0: Formulating the properties of experience and their physical substrate in operational terms. *PLOS Computational Biology*, 20(1):e1011465, 2024. doi: 10.1371/journal.pcbi.1011465.

[11] Ignacio Cea and Camilo Miguel Signorelli. How to be an integrated information theorist without losing your body. *Frontiers in Computational Neuroscience*, 18:1510066, 2024. doi: 10.3389/fncom.2024.1510066.

[12] George A. Mashour et al. An integrative, multiscale view on neural theories of consciousness. *Neuron*, 112(7), 2024. doi: 10.1016/S0896-6273(24)00088-6.

[13] Cryo-em structure of gdp-microtubule co-polymerized with eb3. https://www.rcsb.org/structure/3JAR, 2015. RCSB PDB: 3JAR.

[14] Max Tegmark. Importance of quantum decoherence in brain processes. *Physical Review E*, 61(4):4194–4206, 2000. doi: 10.1103/PhysRevE.61.4194.